Recent global trends in atmospheric fronts

Gareth Berry,[1] Christian Jakob,[1] and Michael Reeder[1]

[1] An automated, objective method is used to identify atmospheric fronts in four independent reanalysis data sets for the period 1989–2009 and to calculate changes in their frequency. The analysis highlights several coherent regions of statistically significant change in the frequency of fronts. The front frequency in the North Atlantic storm track has decreased by about 10–20%, whereas changes observed over the Southern Ocean are relatively small. In the subtropical Pacific the front frequency has increased significantly, which is consistent with an expansion of the dry subtropics. The sensitivity of these trends to the detection method is tested and the results are found to be robust. The results provide a concise summary of the recent changes in a major component of synoptic weather conditions, providing a benchmark for climate models as well as an additional tool for interpreting climate change predictions. **Citation:** Berry, G., C. Jakob, and M. Reeder (2011), Recent global trends in atmospheric fronts, *Geophys. Res. Lett.*, *38*, L21812, doi:10.1029/2011GL049481.

1. Introduction

[2] Atmospheric fronts delineate air masses with different thermal characteristics and are the focus of much of the significant weather in the mid and higher latitudes. These air mass boundaries are frequently associated with precipitation in the mid and higher latitudes and are commonly displayed on weather maps as line features. Since its introduction in the early part of the twentieth century [*Bjerknes*, 1919], the concept of a front has had widespread use in research, weather forecasting, and in communicating such forecasts to the general public. Despite their central importance in the day-to-day weather, their properties on climate timescales has been unexplored to date.

[3] Analyzing the properties of fronts on long timescales is problematic as they are only recorded symbolically on weather charts in the form of discontinuous line segments. Moreover, they are often analyzed subjectively and drawn by hand. Recently, objective methods of drawing fronts from gridded numerical weather prediction data sets have been used to compute front climatologies from reanalysis data sets. Using shifts in the meridional wind field along with automated tracking, *Simmonds et al.* [2011] examined the properties of fronts in the Southern Hemisphere in detail. A global objective climatology of weather fronts in the ECMWF ERA-40 reanalysis data set was constructed by *Berry et al.* [2011] using a thermodynamic front detection technique derived by *Hewson* [1998] coupled to an algo-rithm that detects front locations and joins front points into frontal segments. In the research reported here, the work of *Berry et al.* [2011] is expanded by using the objective front detection algorithms to explore the global trends in atmospheric fronts in recent decades in four independent reanalysis data sets.

2. Methodology and Data Sets

[4] The same technique and parameters for front detection as *Berry et al.* [2011] are adopted here to explore frontal trends, although the analysed fronts are not classified into types (cold/warm etc.) in this study. The location of fronts is defined by several derivatives of a thermodynamic field following the equations described by *Hewson* [1998] and references therein. In essence, the location of a front is defined by how quickly the gradient of the magnitude of the 850-hPa wet bulb potential temperature (θ_w) changes along a moist isentrope. These derivatives produce a two-dimensional field where masks are applied according to threshold values to leave truncated contours corresponding to front locations. This was performed graphically by *Hewson* [1998] and numerically by *Berry et al.* [2011] by grouping individual points into front segments based on their proximity to neighbouring points. Following *Hewson* [1998], the 850-hPa θ_w is selected as the thermodynamic variable, although the sensitivity of the results is examined by repeating the analysis using the 850-hPa potential temperature (θ).

[5] Objective front locations are computed every 6 hours for the period 1989–2009 from four reanalysis data sets: (i) The European Centre for Medium range Weather Forecasts (ECMWF) ERA-Interim (ERAI) reanalysis [*Simmons et al.*, 2007], (ii) the National Centers for Environmental Prediction–Department of Energy reanalysis 2 data set (NCEP2) [*Kistler et al.*, 2001], (iii) the Japanese Meteorological Agency 25-year reanalysis and climate data assimilation system (JRA) [*Onogi et al.*, 2007] and (iv) the NASA Modern Era Retrospective-analysis for Research and Applications (MERRA) [*Bosilovich et al.*, 2006]. Each data set is interpolated to a common 2.5 × 2.5° horizontal grid as the frontal detection algorithm is sensitive to resolution (because it depends on horizontal derivatives) and because it allows the results to be directly compared with [*Berry et al.*, 2011], who use the ECMWF ERA-40 data set.

[6] Annual mean front frequencies are computed and linear regression is used to estimate the trend at each grid point. A robust climate signal is found where the trends in all reanalyses have the same sign and the trends in the individual reanalyses are significant at the 95% level using a two-tailed Student's t-test. Grid points where the topography is above 1.5 km (850 hPa in the standard atmosphere) are excluded. One caveat is that the MERRA reanalysis does not interpolate data below the surface, and consequently, the algorithm truncates the front locations near high terrain as

[1]Monash Weather and Climate, Monash University, Clayton, Victoria, Australia.
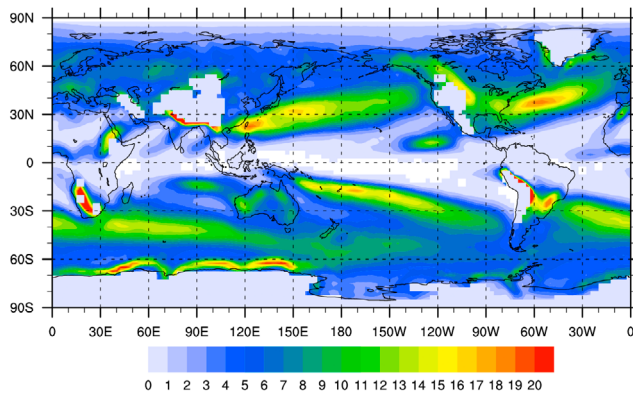
Figure 1. Annual mean front frequency (percentage of analysis times) for the period 1989–2009 averaged over ERAI, NCEP, JRA and MERRA data sets. Values within 1 grid point of terrain exclude the MERRA reanalysis (see section 2 for details).

the scheme uses centred finite differences. In those cases where the MERRA data is unavailable for this reason, the trends are determined from the remaining reanalyses. Additional tests of the robustness of the results and their sensitivity to the method are conducted by varying the thermodynamic parameter (i.e. using both 850-hPa θ and θ_w) and also by repeating the analysis using a minimum thermal front parameter [*Renard and Clarke*, 1965] that is half and double the value used by *Berry et al.* [2011].

3. Results

[7] The annual mean front frequency, defined as the percentage of analysis times at which a front is located in each grid box, for the period 1989–2009 is shown in Figure 1, averaged across all four reanalyses. The individual reanalyses are not shown due to their similarity with one another and this mean. Figure 1 bears a strong resemblance to the ERA-40 frequency reported for the period 1958–2001 [*Berry et al.*, 2011]. High front frequencies, of the order 10%, are located in the extratropical storm tracks in the North Atlantic, North Pacific and Southern Oceans. The easternmost portions of these frequency maxima are positioned further poleward, consistent with the net poleward transport of heat and moisture by the global circulation. Subtropical frequency maxima are also evident in the Pacific basin near the South Pacific Convergence Zone (SPCZ) and near Taiwan; this is presumably a consequence of the mean flow producing sufficiently strong boundaries in moisture and temperature away from the storm tracks [cf. *Hodges et al.*, 2003]. High front frequencies lie close to high terrain, especially at high latitudes (e.g. east of the Canadian Rocky mountains), which are linked to persistent baroclinic zones produced by a change in the underlying surface (e.g. the edge of the Antarctic ice pack).

[8] Using the annually averaged front frequencies from the four reanalyses, the trend over the period 1989–2009 is estimated for each data set separately through linear regression. The average trend, defined as the total percentage change over the 21-year period across all four reanalyses is displayed in Figure 2a, with the 1989–2009 annual mean sea level pressure overlaid for reference. The same

trend data are shown in Figure 2b, except that these data are only displayed where the trends in all four reanalyses have the same sign and where the trend in each reanalysis is significant at the 95% level using a two-tailed Student's T-test. To aid interpretation, contours of annual mean front frequency are overlaid in Figure 2b. These trend maps show that, although a large proportion of the grid points are removed by the statistical tests (primarily the significance level), the remaining field exhibits large contiguous regions where the trends have a coherent structure.

[9] In particular, there has been a decrease of the order 10–20% in front frequency in a large region, between 30–50°N, extending from the United States to central Europe and encompassing much of the North Atlantic storm track [*Hodges et al.*, 2003]. Poleward of these regions there are local increases (e.g. North-Eastern Canada and near Iceland). The positive trends exist primarily where the mean frequencies are small (Figure 1), indicating that fronts in the North Atlantic region have become less common overall. The trends in the Pacific basin are more complex due to the presence of well defined front maxima in both the subtropics and mid-latitudes. In the Northern Pacific, reductions in the mid-latitude front frequency south of Japan and in the Gulf of Alaska are noted. In the mid-latitudes it is expected that fronts serve as a crude proxy for cyclone activity. Thus the results presented here are consistent with a large body of research, which has examined cyclone activity using a variety of methods, including sea level pressure feature tracking [e.g., *McCabe et al.*, 2001; *Wang et al.*, 2006] and dynamical parameters [e.g., *Paciorek et al.*, 2002], finding that the northern hemisphere storm tracks have shifted poleward.

[10] Some of the largest global trends are evident in the subtropical North Pacific. In the vicinity of the northern Philippines, on the poleward flank of the western Pacific warm pool, the front frequency has almost doubled during the analysis period. In the north-eastern Pacific a large positive trend extends across the centre of the mean subtropical anticyclone, consistent with the theorised expansion of the subtropical dry regions (and associated moisture gradients) with increasing global temperature [*Seager et al.*, 2010]. The trends in the southern Pacific are dominated by a dipole close to the front frequency maximum associated with the SPCZ. Here, there are negative trends within the climatological frequency maximum and a similarly sized region of positive trends located to its south west. One interpretation is that the frontal zone corresponding to the SPCZ has shifted position and changed orientation in response to the expansion of the dry subtropics [*Seager et al.*, 2010].

[11] In contrast, the reanalyses show little change in the front frequency over the Southern Ocean; there are very few statistically significant points in the region of the frequency maximum and the percentage changes for those the few are small. In general, Figure 2a suggests that the front frequency over the Southern Ocean is tending to decrease poleward of 60°S and increase equatorward. It has been argued that changes in the latitude of the storm track are controlled by circulation changes arising from tropospheric warming and stratospheric ozone, which oppose one another [*Arblaster et al.*, 2011; *Perlwitz*, 2011], although it should be noted that a paucity of observations in this region may lead to increased uncertainty in the accuracy of the renanalyses. Elsewhere there are large trends away from the climatological
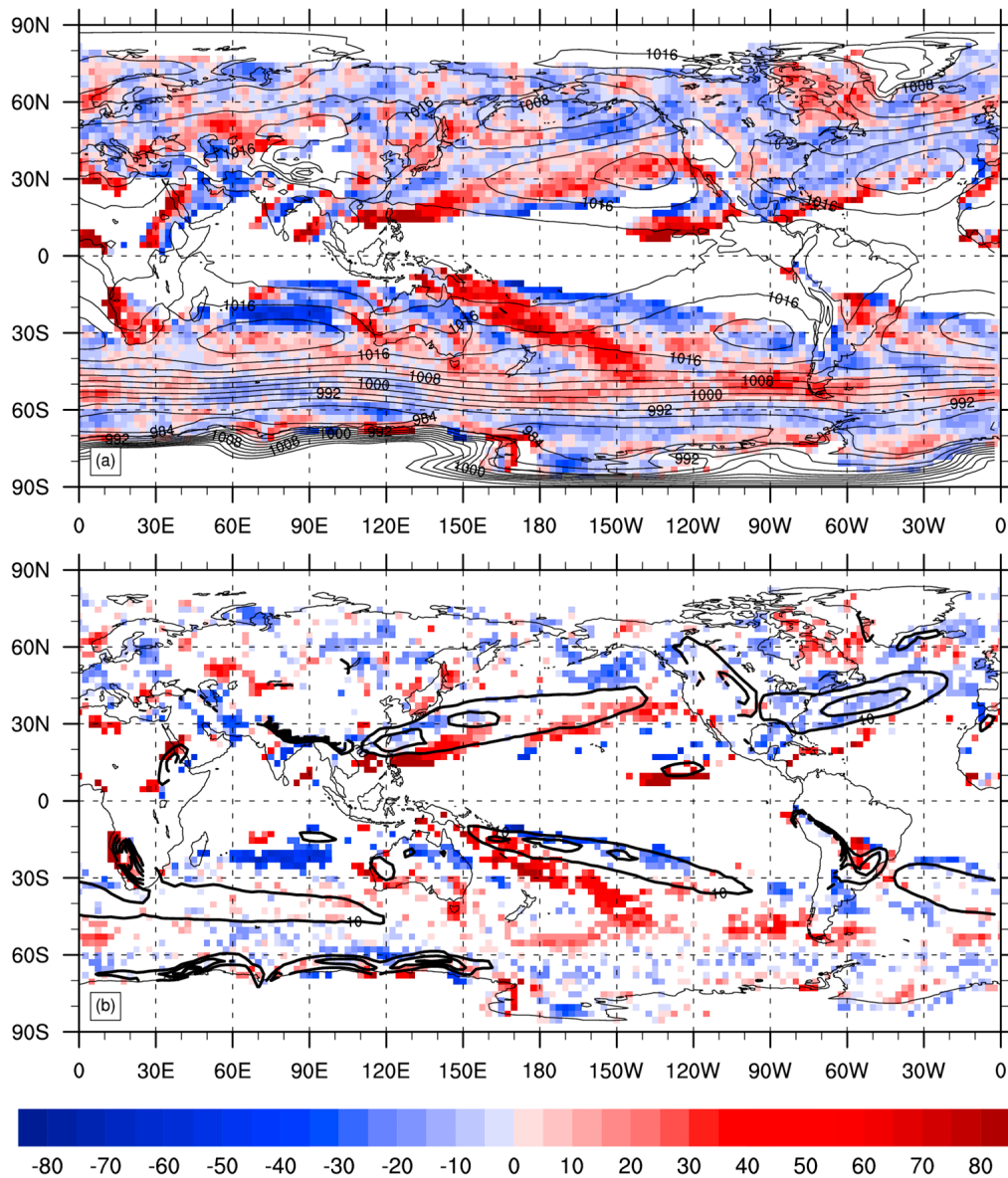
Figure 2. (a) Percentage change in annual mean front frequency 1989–2009, averaged across all reanalyses (ERAI, NCEP2, JRA, MERRA), shown as colours with 1989–2009 mean sea level pressure (drawn every 2 hPa) from the NCEP2 reanalysis overlaid as black contours. (b) Colour shading as in Figure 2a, except trends only shown where all reanalysis trends have the same sign and are individually >95% statistically significant. Contours showing mean frontal frequency every 5% greater than 10% are overlaid. Values within 1 grid point of terrain exclude the MERRA reanalysis.

front frequency maxima (e.g. in the Indian Ocean near 25°S, near the southern tip of South America). Although in these locations there is a large percentage change (and thus important statistically), the trends only signify a relatively small change in the day-to-day weather conditions as the overall number of fronts in these areas is small.

[12] As discussed in the methodology, the automatic computation of front location relies on several derivatives of a thermodynamic field and the application of several threshold-based masks. The thresholds used in constructing Figure 2 were selected by direct comparison with manually generated synoptic maps, which implicitly rely on some conceptual expectation. As it could be argued that the synoptic distinction between a front and more general thermodynamic gra-dient is arbitrary, it is important to demonstrate the same trends exist independently of the threshold choice. Similarly, the numerical properties of the detection algorithm dictate that the thresholds must change in order to provide the same results if the resolution of the input data set is changed, and therefore it is important to prove the trends shown are not predetermined by this. Here, the computation thresholds are changed to test if the trend results presented in Figure 2 are robust. Where the trends are found to be robust, different thresholds will provide insight if the trends shown in Figure 2 tend to be skewed toward changes in more intense or weaker fronts.

[13] The front locations for the period 1989–2009 are recomputed a further two times for each reanalysis using a
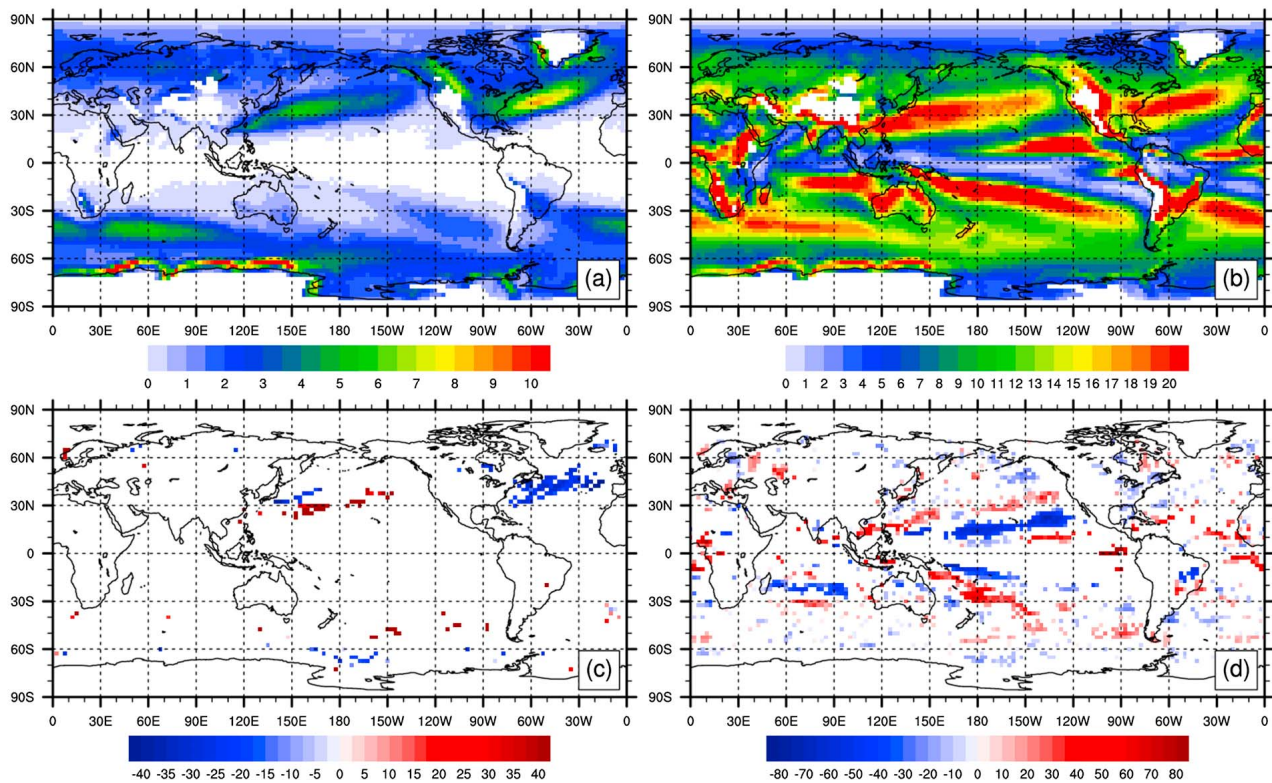
Figure 3. Annual mean front frequency (percentage of analysis times) 1989–2009, averaged across all reanalyses using (a) double the original thermal front parameter (-16×10^{-11} K m^{-2}) and (b) half the original thermal front parameter (-4×10^{-11} K m^{-2}). Also shown are the 1989–2009 percentage change in front frequency where all analyses agree on sign and are >95% statistically significant using (c) doubled original thermal front parameter (-16×10^{-11} K m^{-2}) and (d) half the original thermal front parameter (-4×10^{-11} K m^{-2}). Values within 1 grid point of terrain exclude the MERRA reanalysis (see section 2 for details).

thermal front parameter [*Renard and Clarke*, 1965] that is double and half that used by *Berry et al.* [2011] and in the computation of Figure 2. The mean front frequency and statistically significant linear trends are plotted for these computations in Figure 3. When the threshold is doubled (Figure 3a), the front frequency contracts toward the mid-latitude storm tracks, with very low front frequency within 20° of the equator. Conversely, when the threshold is halved (Figure 3b) the frequency maxima in the midlatitudes are retained, but frequency maxima in the subtropics on the poleward flanks of the Intertropical Convergence Zones (ITCZs) become prominent. This illustrates that the majority of fronts in the subtropics are associated with weak thermodynamic gradients compared to the midlatitudes (consistent with conceptual expectations). Overall, the algorithm produces a consistent climatology with different thresholds.

[14] The trends for fronts computed at different thresholds (Figures 3c and 3d) are also broadly consistent with those already shown in Figure 2. There are only two grid points where the statistically significant trends change sign when recomputed. By comparing the magnitude of the trends computed using the different thresholds, more details about their regional trends can be determined; in particular (Figure 3c) the negative trend in the North Atlantic storm track is most evident at the most stringent threshold i.e. when this is doubled, implying that the overall trend is driven by changes in the more intense fronts. Conversely (Figure 3d),

the front frequency trends at low latitudes (e.g. near the SPCZ) are primarily associated with changes in the frequency of weak fronts.

[15] So far, gradients in the 850-hPa θ_w form the basis of how front are defined, following *Hewson* [1998] and supported by subjective comparison with synoptic weather maps. However, there is no commonly agreed definition and hence, it is possible that other variables maybe better choices [see, e.g., *Simmonds et al.*, 2011]. For this reason the sensitivity of the results presented above to using another thermodynamic variable is explored. If it can be determined that the same basic climatology and trends exist the results presented are robust.

[16] Objective frontal locations are recomputed for the period 1989–2009 using the potential temperature (θ) at 850-hPa in all four reanalysis data sets with the same algorithms described in the methodology section. The θ field was selected for comparison as the water vapor fields used in the computation of trends in Figure 2 (as part of the definition of θ_w) are more uncertain than the temperature fields [*Allan et al.*, 2002]. The resultant climatology and statistically significant trends of the θ and original θ_w computations are shown alongside one another in Figure 4. With the removal of the moisture information, the overall climatology from θ derived fronts (Figure 4b) is similar to that computed using θ_w (Figure 4) with highest frequencies occurring in the mid-latitude storm tracks. Some of the most notable differences in
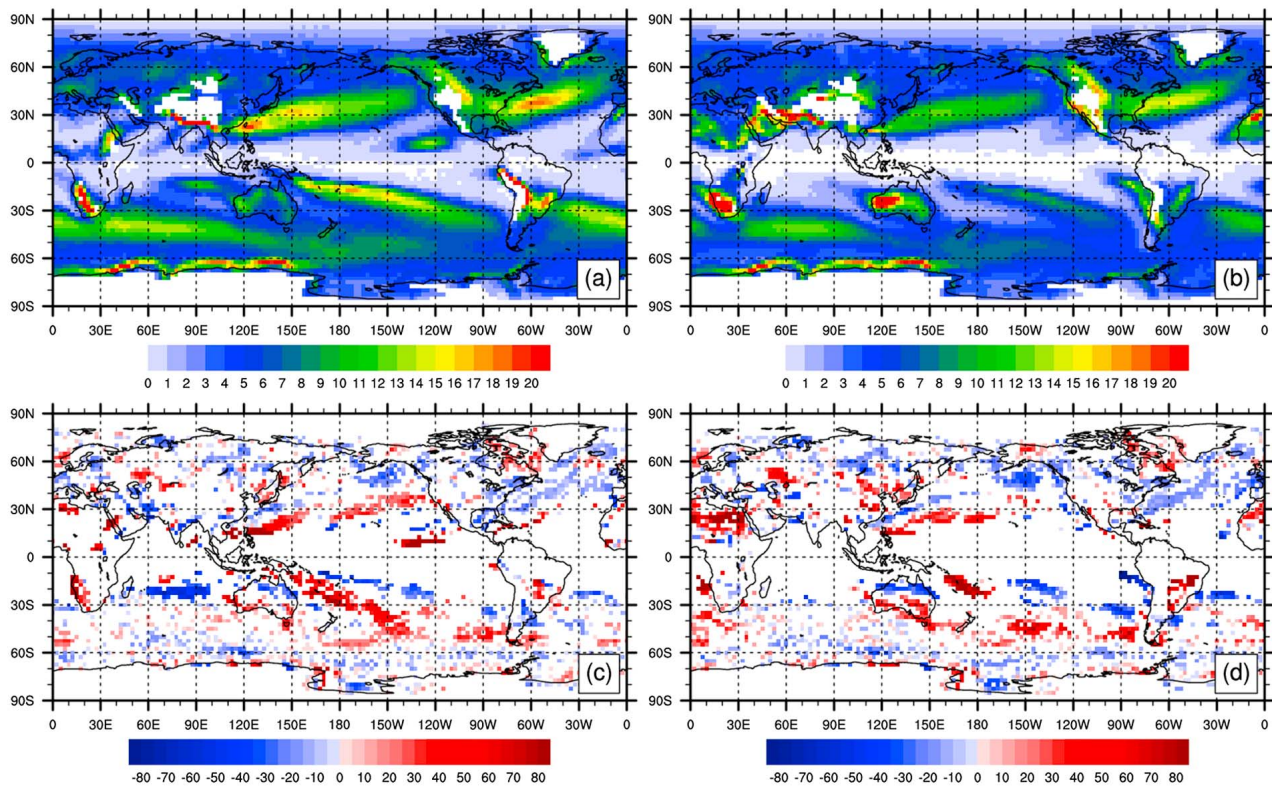
Figure 4. Annual mean front frequency (percentage of analysis times) 1989–2009, averaged across all reanalyses computed using (a) 850 hPa θ_w and (b) 850 hPa θ. Also shown are the 1989–2009 percentage change in front frequency where the trends are >95% statistically significant using (c) 850 hPa θ_w and (d) 850 hPa θ.

the front frequency occur in the subtropics, particularly near the SPCZ, where there are substantial reductions in frequency when θ is used. This signifies that subtropical fronts tend to be strongly associated with moisture gradients. As might be anticipated, large differences in the climatological frequency occur near regions of low humidity and high temperature contrasts, such as the desert regions of Australia and the Middle East, as the west coast of South America where cold upwelling is prominent at the ocean surface. The broad trends shown in the θ_w based analysis (Figure 4c) are also evident in fronts derived from the θ field (Figure 4d). Overall, only 3% of the grid points that have a statistically significant trend in the θ_w analysis change sign in the θ computation and of these two-thirds are found within 30° of the equator. The consistency between results utilising different thermodynamic parameters shows not only that the technique is robust and increases confidence in the overarching conclusions, but provides information as to whether front trends at a specific point are influenced mostly by temperature or moisture changes.

4. Conclusions

[17] Using an objective detection methodology the climatology and trends in the frequency of lower tropospheric fronts have been explored in four modern, independent reanalysis data sets. The annual average front frequencies across the data sets were practically identical to one another and to the ERA-40 climatology reported by [*Berry et al.*, 2011]. Analysis of the trends in the frontal frequency iden-

tified statistically significant and consistent trends within climatological front frequency maxima. In particular, the front frequency in the North Atlantic storm track has decreased by about 10–20%, consistent with the observed poleward shift in the observed storm tracks [e.g., *Paciorek et al.*, 2002; *McCabe et al.*, 2001], whereas few statistically significant trends exist in the Southern Hemisphere mid-latitude storm track. Significant trends are noted in the subtropics, particularly in the Pacific Basin; in these regions front frequency has tended to increase on the flanks of oceanic warm pools and is linked to an increase in the frequency of relatively weak (Figure 3) fronts that are strongly associated with moisture gradients (Figure 4). Such a pattern is consistent with an expansion of the dry subtropics, but could also be explained by more frequent or more intense El Nino events occurring in the latter part of the data record. The trend analysis shown here is limited to a 21-year period in the post satellite era, primarily due to the availability of reanalysis data. When interpreting the results, it should be remembered that variability on long (multi-decadal) timescales has not been captured.

[18] The robustness of these frontal trends has been explored by combining four independent reanalysis products and applying the criteria that the trends at each grid point must have the same sign and are statistically significant in each data set. This rigorous standard ensures that uncertainty is minimised and that any bias or weaknesses in the individual data sets do not influence the main results. A fundamental assessment of the methodology was conducted by repeating the analysis with varying thresholds and by changing the

thermodynamic variable. This analysis showed that not only is the technique is robust and increases confidence in the overarching conclusions, but provides information about the nature of the trend at each point.

[19] Although fronts, rainfall and temperature changes are coupled, synoptic experience shows that there is a strong regional and seasonal dependence, e.g. a springtime cold front in the USA may be a focus for severe convection, whereas a summertime cold front over Northern Australia may only mark a humidity change. For further comment on the consequences of these frontal trends, links between the local weather conditions (e.g. rainfall) must be formalised. With this type of knowledge it will be possible to examine how fronts are predicted to change in the future climate and their quantify their likely impact around the globe.

References

Allan, R. P., A. Slingo, and V. Ramaswamy (2002), Analysis of moisture variability in the European Centre for Medium-Range Weather Forecasts 15-year reanalysis over the tropical oceans, *J. Geophys. Res.*, *107*(D15), 4230, doi:10.1029/2001JD001132.

Arblaster, J. M., G. A. Meehl, and D. J. Karoly (2011), Future climate change in the Southern Hemisphere: Competing effects of ozone and greenhouse gases, *Geophys. Res. Lett.*, *38*, L02701, doi:10.1029/2010GL045384.

Berry, G. J., M. J. Reeder, and C. Jakob (2011), A global climatology of atmospheric fronts, *Geophys. Res. Lett.*, *38*, L04809, doi:10.1029/2010GL046451.

Bjerknes, J. (1919), On the structure of moving cyclones, *Geofys. Publ.*, *1*, 1–9.

Bosilovich, M. G., et al. (2006), NASA's modern era retrospective-analysis for research and applications, *U.S. CLIVAR Variations*, *4*(2), 5–8.

Hewson, T. D. (1998), Objective fronts, *Meteorol. Appl.*, *5*, 37–65, doi:10.1017/S1350482798000553.

Hodges, K. I., B. J. Hoskins, J. Boyle, and C. Thorncroft (2003), A comparison of recent reanalysis datasets using objective feature tracking: Storm tracks and tropical easterly waves, *Mon. Weather Rev.*, *131*(9), 2012–2037, doi:10.1175/1520-0493(2003)131<2012:ACORRD>2.0.CO;2.

Kistler, R., et al. (2001), The NCEP–NCAR 50-year reanalysis: Monthly means CD-ROM and documentation, *Bull. Am. Meteorol. Soc.*, *82*, 247–267, doi:10.1175/1520-0477(2001)082<0247:TNNYRM>2.3.CO;2.

McCabe, G. J., M. P. Clark, and M. C. Serreze (2001), Trends in Northern Hemisphere surface cyclone frequency and intensity, *J. Clim.*, *14*, 2763–2768, doi:10.1175/1520-0442(2001)014<2763:TINHSC>2.0.CO;2.

Onogi, K., et al. (2007), The JRA-25 reanalysis, *J. Meteorol. Soc. Jpn.*, *85*, 369–432, doi:10.2151/jmsj.85.369.

Paciorek, C. J., et al. (2002), Multiple indices of Northern Hemisphere cyclone activity, winters 1949–99, *J. Clim.*, *15*, 1573–1590, doi:10.1175/1520-0442(2002)015<1573:MIONHC>2.0.CO;2.

Perlwitz, J. (2011), Tug of war on the jet stream, *Nat. Clim. Change*, *1*, 29–31, doi:10.1038/nclimate1065.

Renard, R. J., and L. C. Clarke (1965), Experiments in numerical objective frontal analysis, *Mon. Weather Rev.*, *93*, 547–556, doi:10.1175/1520-0493(1965)093<0547:EINOFA>2.3.CO;2.

Seager, R., N. Naik, and G. A. Vecchi (2010), Thermodynamic and dynamic mechanisms for large-scale changes in the hydrological cycle in response to global warming, *J. Clim.*, *23*, 4651–4668, doi:10.1175/2010JCLI3655.1.

Simmonds, I., et al. (2011), Identification and climatology of Southern Hemisphere mobile fronts in a modern reanalysis, *J. Clim.*, doi:10.1175/JCLI-D-11-00100.1, in press.

Simmons, A. S., et al. (2007), ERA-Interim: New ECMWF reanalysis products from 1989 onwards, *ECMWF Newsl.*, *110*, 25–35.

Wang, X. L., et al. (2006), Climatology and changes of extratropical cyclone activity: Comparison of ERA-40 with NCEP–NCAR reanalysis for 1958–2001, *J. Clim.*, *19*, 3145–3166, doi:10.1175/JCLI3781.1.

G. Berry, C. Jakob, and M. Reeder, Monash Weather and Climate, Monash University, Clayton, Vic 3800, Australia. (Gareth.Berry@monash.edu)